

# Acquisition through My Eyes and Steps: A Joint Predictive Agent Model in Egocentric Worlds

Lu Chen<sup>1\*</sup> Yizhou Wang<sup>2\*</sup> Shixiang Tang<sup>2†</sup> Qianhong Ma<sup>3</sup> Tong He<sup>4</sup>  
Wanli Ouyang<sup>2</sup> Xiaowei Zhou<sup>1</sup> Hujun Bao<sup>1</sup> Sida Peng<sup>1†</sup>

<sup>1</sup>State Key Lab of CAD&CG, Zhejiang University <sup>2</sup>The Chinese University of Hong Kong

<sup>3</sup>Shanghai Jiao Tong University <sup>4</sup>Shanghai Artificial Intelligence Laboratory

\*Equal contribution †Corresponding author

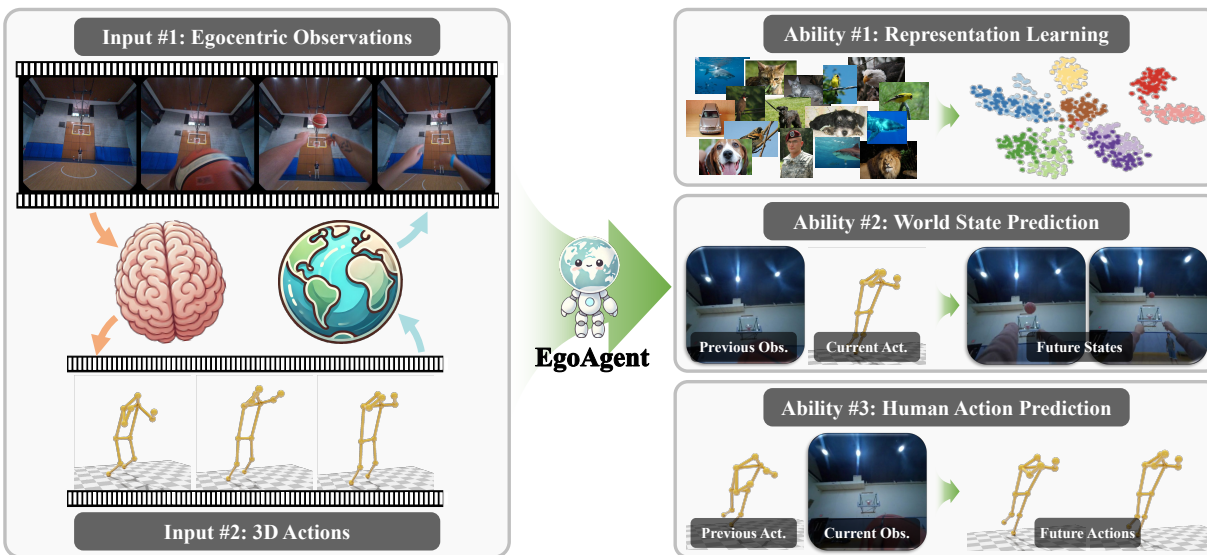


Figure 1. (a) Humans learn from the world by continuously perceiving the egocentric world, predicting future states, and taking actions to achieve their goals. (b) Inspired by the human learning process, we proposed EgoAgent, a joint predictive agent model in egocentric worlds that can learn to represent, predict, and act from egocentric video and 3D human skeleton sequences.

## Abstract

This paper addresses the task of learning an agent model behaving like humans, which can jointly perceive, predict, and act in egocentric worlds. Previous methods usually train separate models for these three abilities, leading to information silos among them, which prevents these abilities from learning from each other and collaborating effectively. In this paper, we propose a joint predictive agent model, named EgoAgent, that simultaneously learns to represent the world, predict future states, and take reasonable actions with a single transformer. EgoAgent unifies the representational spaces of the three abilities by mapping them all into a sequence of continuous tokens. Learnable query tokens are appended to obtain current states, future states, and next actions. With joint supervision, our agent model establishes the internal relationship among these three abilities

and effectively mimics the human inference and learning processes. Comprehensive evaluations of EgoAgent covering image classification, egocentric future state prediction, and 3D human motion prediction tasks demonstrate the superiority of our method. The code and trained model will be released for reproducibility.

## 1. Introduction

This paper aims to build an agent model, as defined by David Ha and Jurgen Schmidhuber [25], inspired by the human cognition system. Built upon world models that focus on predicting the environment, the agent model contains an additional action proposal component, emphasizing the capability to take actions in response to predicted states. Motivated by the acquisition process of human commonsense,

we design our agent model to take egocentric RGB observations as input and learn to perceive, predict, and interact with the world. Such abilities are essential for applications in robotics, gaming, and virtual reality, where the agent needs to understand what is happening in the world, anticipate what will happen next, and decide what actions to take to achieve its objectives. It is challenging to build a model that can possess these three abilities like humans, considering two key aspects. First, the three abilities of humans are closely intertwined, where perception and prediction provide information for interaction, and interaction allows the model to better understand the world. Second, the learning of these three abilities is also closely related. Humans develop internal models of the world through an ongoing cycle of perception and interaction, which reinforce each other.

Previous methods typically focus on building one of the three abilities, with typical vision tasks including (1) Visual representation learning [10, 12, 29, 32, 50], which encodes high-level states of human observations, *i.e.*, images and videos; (2) Action prediction [9, 40], which forecasts future human actions according to past actions; (3) World model [41, 57], which predict world state transitions based on observations and actions. However, we argue that training separate models for perception, prediction, and interaction leads to information silos between the models, preventing them from learning from each other and collaborating effectively. It is crucial to establish the relationship between these three abilities, allowing them to reinforce each other in both inference and learning processes.

In this paper, we propose a novel joint predictive agent model in egocentric worlds, named *EgoAgent*, that simultaneously learns to represent world observations, predict future states, and act based on learned representations (Figure 1). Our core innovation lies in a single transformer that unifies the representational spaces of the three abilities by mapping them into a sequence of continuous tokens. Specifically, given egocentric observations and historical human actions, we map them into high-dimensional feature vectors using projection layers. Then, these feature vectors are fed into a transformer along with a set of pre-defined query tokens to obtain the current state features, future state features, and the following actions. We adopt a teacher-student mechanism to train the agent model, which jointly learns visual representation extraction, future state prediction, and action prediction.

Our unified agent model brings three benefits. First, thanks to the attention mechanism of the transformer, our model naturally establishes internal relationships among the three abilities. Second, aligning representation space allows the transformer to be compatible with multi-modal data and maintain full parameter-sharing, increasing training samples for three sub-tasks. Third, our proposed model enables us to leverage the task of action generation to reinforce the

learning of world perception and future prediction, effectively mimicking the human learning process.

Extensive experiments on egocentric video and human motion dataset [21] demonstrate that *EgoAgent* can well handle tasks on perception, prediction, and action, even pushing the performance limits of the existing state-of-the-art methods. Specifically, *EgoAgent* outperforms the leading egocentric video pretraining method [47] by **+1.40%** and **+1.32%** Top1 accuracy on ImageNet-100 and ImageNet-1K for the image classification task, **+16.28%** Top1 accuracy and **+16.95%** mAP on Ego-Exo4D [21] future state prediction task, respectively. Furthermore, on the 3D human motion prediction task, *EgoAgent* surpasses both video-based motion generation models and motion prediction methods, achieving **-0.82** MPJPE (cm) performance improvement at 30 fps prediction rate.

Our contributions are two-fold: (1) We develop a joint predictive agent model in egocentric worlds named *EgoAgent*, which can simultaneously learn to represent the observation, predict future states, and generate informed actions. (2) We evaluate our *EgoAgent* on egocentric video-action datasets and show its superior abilities in image classification, egocentric future status prediction, and 3D human motion prediction tasks.

## 2. Related Work

### 2.1. Egocentric Visual Representation Learning

Traditional visual representation methods learn the features on large-scale curated image datasets, *e.g.*, ImageNet [16], using supervised [27, 32, 50] or self-supervised methods [10, 12, 28]. As curated datasets consume lots of resources, which limits the training scale, researchers turn to more accessible data, *i.e.*, egocentric videos. R3M [42] and VIP [36] captured the temporal relationships among egocentric videos, learning generic representations on Ego4D [20] for robotics. Recently, Venkataramanan et al. [47] proposed DoRA to learn object-level representation on their proposed egocentric video dataset, WalkingTours. Aiming to mimic the process of how humans learn from the egocentric world, we proposed a joint predictive agent model that can not only learn representative features using egocentric videos but also predict future states and generate informed actions.

### 2.2. World Models

World models aim to predict future world states based on previous observations and actions. These models can be broadly classified into two main categories: generative and predictive models. Generative world models [2, 25, 53] often employ an autoencoder framework, training to capture state transitions within the input image or video space. Recently, these models have demonstrated success in applica-

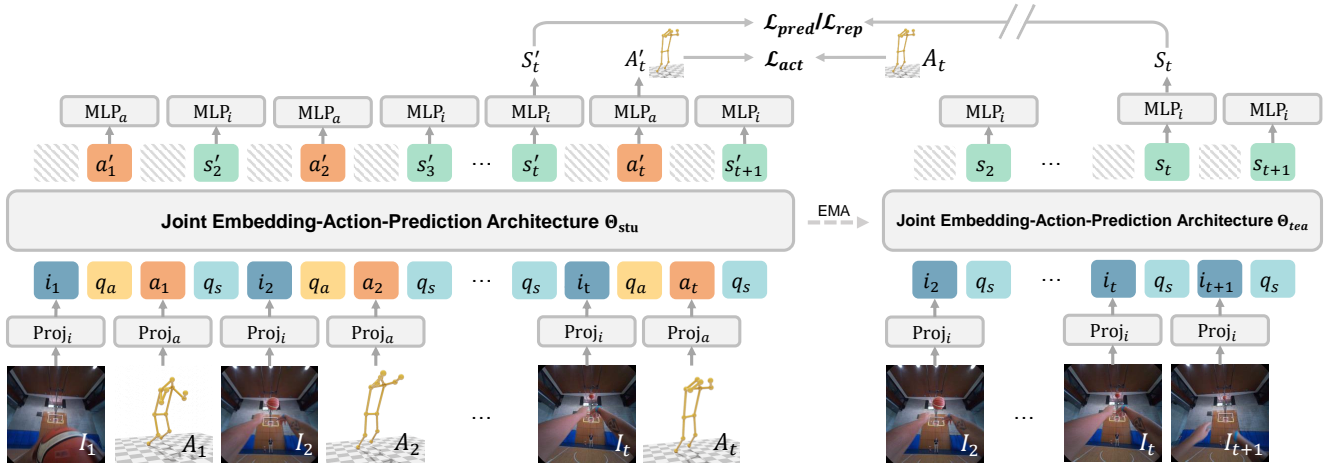


Figure 2. The overall framework of EgoAgent. EgoAgent adopts the Joint Embedding-Action-Prediction Architecture to embed input egocentric video frames and 3D human pose sequences into image tokens  $i$  and action tokens  $a$  with corresponding projectors respectively. Learnable action query token  $q_a$  and future state query token  $q_s$  are appended after the image and action tokens to stimulate EgoAgent to predict the next action  $A'$  and scene state  $S'$ . An action prediction loss  $\mathcal{L}_{act}$  is adopted to guide the training process of image-based action anticipation. Since EgoAgent predicts scene states  $S'$  in an image feature space, the target future state  $S$  is obtained from a momentum teacher network  $\Theta_{tea}$ . Features from the student and teacher branches are aligned through a state prediction loss  $\mathcal{L}_{pred}$ . When 3D skeleton sequences are not paired with the video, EgoAgent randomly crops different views from egocentric observations and learns representative features only with image tokens  $i$  and state query tokens  $q_s$  by a representation loss  $\mathcal{L}_{rep}$ . For easier understanding, we only illustrate the supervisions on predicting the scene state and action at time step  $t$ .

tions such as autonomous driving [51], robotics [24], and game control [5]. Notably, GAIA-1 [30] mapped multimodal driving signals into discrete tokens, which are then encoded into a unified representation using an autoregressive transformer. UniSim [57] learned a universal simulator from diverse human demonstrations for robotic manipulation with a diffusion model. Predictive world models [3, 7, 19, 33] focus on capturing the dependencies between two action-connected states without explicitly generating images or videos. MC-JEPA [6] encompassed self-supervised learning with optical flow estimation to jointly learn content features and motion information. SWIM [41] utilized large-scale Internet human videos to pretrain a world model to build a structured action space for robots.

### 2.3. 3D Human Motion Prediction

Human motion prediction models [34, 48, 55] aim to forecast future body movements given historical poses. Aksan et al. [1] proposed a transformer-based architecture to capture spatial-temporal dependencies of human motion over short and long horizons. Cui et al. [15] represents the human skeleton as a dynamic graph to adaptively learn joint connection strengths for better prediction accuracy. Other works [37, 58] incorporate physics-based priors, such as inverse kinematics, to ensure the generated motions adhere to physical principles. Recent research has integrated multimodal cues like textual instructions [39], eye gaze [59], and 3D objects [56] as conditions for human motion prediction. A growing body of works [14, 26, 49] highlighted

the importance of scene-awareness in this task. Notably, Cao et al. [9] proposed a three-stage framework that consists of goal prediction, path planning, and pose finalization, effectively leveraging scene context to enhance goal-oriented motion prediction.

## 3. Method

Given the egocentric observations and history human actions, our paper aims to learn an agent model that can represent the scene state, predict future states, and predict the following actions. As humans learn to understand the world’s underlying dynamics by observing and interacting with it, we believe these three tasks share internal relations, so that can be jointly learned and be beneficial to each other.

The overview of our proposed architecture is presented in Figure 2. We first introduce the base model of our joint embedding-action predictive architecture and describe how to represent the current scene state, predict future scene state and human action with the base model (Section 3.1). Then, we introduce how it can be learned in Section 3.2. Finally, we demonstrate the applications of our agent model in various tasks in Section 3.3.

### 3.1. Joint Embedding-Action-Prediction Architecture for EgoAgent Model

**Base model.** We employ a Large Language Model (LLM) [4, 31, 43–45] as the foundational architecture for our agent model and adapt it to jointly predict future scene

states and human actions, as well as to extract image features. This design choice is motivated by two main reasons. First, our objective of near-future world prediction aligns closely with LLMs’ inherent next-token prediction capability. Second, the well-structured and straightforward architecture of LLMs provides a flexible and extensible foundation for our specific tasks.

In practice, we adopt the InternLM [44] as the backbone, with adjustments made to the input and output formats: we modify the input to be the observed images and actions, and the output to be the scene states and human actions. To accommodate these changes, we adapt relevant network layers accordingly. Notably, instead of using pretrained tokenizers like VQVAE [46] to convert images and actions into discrete tokens, we utilize learnable convolutional layers to project them into continuous feature representations.

**Jointly predict and act.** Given egocentric observations  $V = \{I_0, I_1, \dots, I_t\}$  and history human actions  $A = \{A_0, A_1, \dots, A_t\}$ , our agent model aims to predict the future scene state  $S_{t+1}$  corresponding to the anticipated observation  $I_{t+1}$  and to generate plausible human action  $A_{t+1}$  by understanding the current scene state  $S_t$  at the same time. The scene state is represented as a set of high-dimensional feature vectors, whereas the human actions are represented as sequences of 3D human skeletons. In contrast to previous methods [8, 53, 57] that represent the scene states using raw images or videos, our feature vector embedding allows the model to focus on higher-level concepts. This abstraction aligns more closely with human perception and predictive process in the real world, as highlighted in IWM [19].

Specifically, we begin by encoding the egocentric video  $V$  and human action sequence  $A$  into feature vectors. For egocentric video, following a similar approach to ViT [17], we use a convolutional layer to process each video frame  $I_t$ , producing a feature map that is then subdivided into a set of image feature vectors. These features are flattened to form the input image tokens  $i_0, i_1, \dots, i_t$ . For human actions, we utilize a convolutional layer with a Layer Normalization (LN) and a Gaussian Error Linear Unit (GeLU) activation layer to map the human skeletons  $A_t$  into action features  $a_t$ . The Transformer network within the LLM then processes these feature vectors to produce the target outputs. As illustrated in Figure 2, the input sequence is formatted as a sequence of image, action, and query tokens, in line with LLM practices. Different from text index tokens, our tokens are continuous feature vectors.

At each time step  $t$ , we assemble a fragmented sequence of tokens, including image tokens  $i_t$ , an action query token  $q_a$ , action tokens  $a_t$ , and a future state query token  $q_s$ , where the query tokens are represented as learnable embeddings. The future state query token  $q_s$  prompts the model to take previous image tokens  $i_{0:t}$  and action tokens  $a_{0:t}$  into consideration. Notably, similar to next-token prediction, we

insert the action query token  $q_a$  right after the image tokens  $i_t$  and before the input action tokens  $a_t$ , ensuring that the model relies solely on past observations and actions to predict subsequent actions. Subsequently, the transformer network processes the input token sequence and outputs action embeddings  $a'_t$  and future state embeddings  $s'_{t+1}$  in response to the query tokens. Finally, we utilize separate MLP networks to map these embeddings to the predicted actions  $A'_t$  and future scene states  $S'_{t+1}$ .

### 3.2. Learning EgoAgent in Feature Space

**Asymmetric feature branch.** Similar to IWM [19], we train our agent model at the feature level. To this end, we introduce an additional asymmetric feature branch as a teacher network, which extracts only image features and provide guidance for the student branch, as illustrated in Figure 2. Thanks to the flexible structure of the LLM architecture, this feature branch can be easily implemented by adjusting the network input to a reduced sequence of image tokens  $i_t$  and a state query token  $q_s$  compared to the main network. The model then outputs a world state represented as an image embedding, which is fed into an MLP network to obtain the scene state feature  $S_t$ .

**Supervisions for predicting scene states and actions.** The student branch predicts the future world states  $S'_{t+1}$  and actions  $A'_t$ , while the asymmetric feature branch (teacher) takes only the egocentric image  $I_{t+1}$  to extract the future scene states  $S_{t+1}$ . Given the input token sequence at time step  $t$ , the loss function for training the model to predict future states and actions is defined as:

$$\mathcal{L}_{act}(t) = \mathcal{L}_1(A'_t, A_t), \quad (1)$$

$$\mathcal{L}_{pred}(t) = \mathcal{L}_{dino}(S'_{t+1}, sg[S_{t+1}]), \quad (2)$$

where  $sg[\cdot]$  denotes the stop-gradient operation,  $\mathcal{L}_1$  and  $\mathcal{L}_{dino}$  represent the L1 loss and the DINO loss [10], respectively. Following common practices in self-supervised learning [10, 28],  $sg[\cdot]$  is applied to block the gradients from back-propagating to the teacher branch. The weights of the teacher branch are updated in each iteration using an Exponential Moving Average (EMA) of the student branch.

**Self-supervision for learning powerful representations.** When humans learn to interact with the environment, they first develop an understanding of the observed scene and objects, which then aids them in predicting future states of the world and making appropriate responses. Inspired by this process, we introduce an additional self-supervised learning loss on EgoAgent to facilitate learning representative features from egocentric videos from scratch:

$$\mathcal{L}_{rep}(t) = \mathcal{L}_{dino}(\Theta_{stu}(I_t^{v1}), \Theta_{tea}(I_t^{v2})). \quad (3)$$

Here,  $\Theta_{stu}$  and  $\Theta_{tea}$  denote the student and teacher networks of EgoAgent, respectively,  $I_t^{v1}$  and  $I_t^{v2}$  denote the



two different views derived from the egocentric image  $I_t$ .

**Overall objective function.** Given an input token sequence containing  $t$  time steps, we have the overall objective function  $\mathcal{L}$  defined as:

$$\mathcal{L} = \frac{1}{t} \sum_{k=0}^t (\lambda_{rep} \mathcal{L}_{rep} + \lambda_{pred} \mathcal{L}_{pred} + \lambda_{act} \mathcal{L}_{act}), \quad (4)$$

where  $\lambda_{rep}$ ,  $\lambda_{pred}$ , and  $\lambda_{act}$  are the corresponding loss weights for representing the world, predicting future scene states and actions, respectively.

### 3.3. Applications

After training, EgoAgent inherently possesses three valuable applications.

**Visual representation learning:** EgoAgent learns scene states as feature representations, allowing it to extract meaningful features from input images by  $S = \Theta(I)$ , where  $\Theta$  denotes the EgoAgent model. These features can be directly applied to representation tasks, *e.g.*, image classification.

**Future state prediction:** given egocentric video clips with historical human action sequence, EgoAgent is capable of predicting future scene states  $S_{t+1}$  by  $S_{t+1} = \Theta(I_0, A_0, \dots, I_t, A_t)$ . Once predicted, the future scene image can then be retrieved by measuring similarity within the learned feature space, enabling applications that require foresight into upcoming visual states.

**Human action prediction:** from an egocentric perspective and informed by previous actions, EgoAgent can generate plausible future human actions  $A_t$  as a sequence of 3D skeletons by  $A_t = \Theta(I_0, A_0, \dots, A_{t-1}, I_t)$ . This predictive capability is essential for applications in humanoid robotics, virtual environments, and interactive gaming, where anticipating human-like movements is crucial.

## 4. Experiments

### 4.1. Datasets

As humans perceive the world through the first-view perspective, to imitate the learning process of humans, we train the proposed EgoAgent on two egocentric video datasets, *i.e.*, WalkingTours (WT) [47] and Ego-Exo4D [21]. WT is a video-only dataset, which comprising approximately 1.5 million high-resolution frames captured in various cities worldwide. Ego-Exo4D has 221.26 egocentric video hours with 5035 takes, accompanied by 376K manually labeled 3D body poses and 9.2M automatically generated 3D body poses. We undistort the raw sensor data captured from fish-eye cameras into pinhole cameras to eliminate the imaging projection difference between Ego-Exo4D and WT. We apply a 20-frame sliding window filter to ensure continuous pose sequences, resulting in 1,410,119 clips with synchronized egocentric videos and 3D body poses. Based on the

Table 1.  $k$ -NN evaluation results on ImageNet-100 and ImageNet-1K. Top1 and Top5 accuracy (%) are reported.

Method	Training Dataset	ImgNet-100		ImgNet-1K	
		Top1	Top5	Top1	Top5
<i>Representation Models</i>					
R3M [42]	Ego4D	4.82	14.42	0.77	0.77
VIP [36]	Ego4D	8.04	21.14	1.59	1.59
DINO [10]	WT	-	-	31.1	-
DoRA [47]	WT	55.08	78.06	34.52	52.50
<i>World Models</i>					
OpenSora (V1.1)	Hybrid Dataset	33.44	58.4	16.03	29.05
<i>Agent Models</i>					
EgoAgent-300M	WT+Ego-Exo4D	55.14	76.56	34.65	51.42
EgoAgent-1B	WT+Ego-Exo4D	<b>56.48</b>	<b>78.12</b>	<b>35.84</b>	<b>53.03</b>

EgoPose division in Ego-Exo4D, we reserve the validation set of Ego-Exo4D-v2<sup>1</sup> for evaluation and use the remaining clips for training, yielding 1,378,672 training clips and 31,447 evaluation clips.

### 4.2. Implementation Details

To alleviate the training burden, we sample one image frame every 5 frames from the video clips, while keeping all 3D body skeletons. Specifically, for each clip with 20 frames, we divide it into  $T_s = 4$  time steps and sample the first image frame from each time step. This results in every time step consisting of one image frame paired with five frames of 3D body poses. For representation learning on egocentric videos, we follow the practice in [47] to avoid cropping noisy positive pairs. Following DINO [10], we adopt two global crops and six local crops.

We use InternLM as the backbone in all our experiments. Following the configurations in [22], we train EgoAgent with two model sizes, *i.e.*, InternLM-300M and InternLM-1B. We adopt the same Adam optimizer as that in InternLM with  $\beta_1 = 0.9$ ,  $\beta_2 = 0.999$ . We train EgoAgent on the datasets for 72,000 iters with a linear warm-up of 1800 iters. We set the base learning rate to  $6 \times 10^{-4}$  with a cosine decay scheduler. The loss weights are set as  $\lambda_{rep} = 2$ ,  $\lambda_{pred} = 1$ ,  $\lambda_{act} = 3$ , respectively. All models are trained from scratch using FP16 to speed up. The whole training takes 25, 60 hours in total with a batch size of 1920 on 32, 48 NVIDIA A100 GPUs for EgoAgent-300M, and EgoAgent-1B, respectively.

### 4.3. Represent: Image Classification

We examine the representative capability of EgoAgent, measuring the performance of classification on ImageNet-100 and ImageNet-1K [16] by  $k$ -NN. Concretely, we freeze the model and extract features of images from

<sup>1</sup>The whole Ego-Exo4D dataset is divided into Ego-Exo4D-v1 and Ego-Exo4D-v2 on the original website (<https://ego-exo4d-data.org>).

Table 2. Feature retrieval results on predicted features of the next frame and features extracted from the next frame. Averaged Top-1 accuracy and mAP on total timesteps  $T_s = 4$  are reported.

Method		Training Dataset	Top1	mAP
Representation	VIP [36]	Ego4D	1.67	6.10
	R3M [42]	Ego4D	24.42	37.26
	DINO [10]	WT	28.24	43.42
	DoRA [47]	WT	30.15	45.01
Agent Models	EgoAgent-300M	WT+Ego-Exo4D	43.01	58.06
	EgoAgent-1B	WT+Ego-Exo4D	<b>46.43</b>	<b>61.96</b>

train/validation sets, then utilize a  $k$ -nearest neighbor classifier with  $k = 20$ .

**Results.** As illustrated in Table 1, trained on egocentric videos from scratch, our EgoAgent achieves the best representation performance. Specifically, EgoAgent-1B outperforms DoRA by **+1.40%** and **+1.32%** Top1 accuracy on ImageNet-100 and ImageNet-1K, respectively, demonstrating that the task of representing the world can be well integrated into learning of world models. Notable, compared with OpenSora, which adopts a much larger dataset ( $\times 3$  of EgoAgent training set) for training, EgoAgent-1B shows remarkable performance improvement (**+19.81%**) on ImageNet-1K Top1 accuracy. This indicates that learning a world model on the feature space is more effective for learning powerful representations than on the latent space.

#### 4.4. Predict: Egocentric Future State Prediction

To evaluate the effectiveness of EgoAgent in predicting future states of the world, we perform an egocentric video prediction task with feature retrieval. Specifically, given the egocentric frame and 3D human skeleton sequences as actions at the current time step, the query set stores the features of the egocentric frame at the next time step predicted by models, while the gallery set contains the features directly extracted from the next frames. At the time step  $t$ , if the predicted future state  $S'_{t+1}$  in the query set can correctly retrieve scene state  $S_{t+1}$  features in the gallery, we treat it as a successful future state prediction. For representation models, there are no actions to modify the input image features, the predicted future state  $S'_{t+1}$  is exactly the scene state  $S_t$  at time step  $t$ . To avoid retrieving the exact same features, when querying with input image  $I_t$ , we ignore the scene state  $S_t$  in the gallery set. Following common practice in retrieval tasks, we use Top1 accuracy and mAP as metrics.

**Results.** We summarize the egocentric future state prediction results in Table 2. First, EgoAgent outperforms representation models by a large margin. Concretely, EgoAgent-300M improves the performance of DoRA by **+12.86%** Top1 accuracy and **+13.05%** mAP, showing that EgoAgent predicts the future states not only based on semantic simi-

Table 3. 3D human motion prediction results on Ego-Exo4D. We provide the results of predicting human skeletons with a time gap of 1/30 and 1/10 seconds, respectively. MPJPE and MPJVE are in cm and cm/s, respectively.

Method	Predict@30fps		Predict@10fps	
	MPJPE↓	MPJVE↓	MPJPE↓	MPJVE↓
<i>Video-based Motion Generation Models</i>				
Diffusion Policy-C [13]	28.07	206.96	27.95	114.75
Diffusion Policy-T [13]	25.92	353.24	25.85	148.82
<i>Motion Prediction Models</i>				
HumanMAC [11]	19.21	94.22	17.68	77.43
siMLPe [23]	13.33	81.94	12.2	60.65
<i>Agent Models</i>				
EgoAgent-300M	12.92	82.18	11.89	59.96
EgoAgent-1B	<b>12.51</b>	<b>81.45</b>	<b>11.65</b>	<b>58.99</b>

ilarity. On the contrary, representation models can only retrieve future state features using semantic similarity, making it hard for them to deal with visually similar frames in egocentric videos. Second, EgoAgent-1B achieves further performance gains on EgoAgent-300M with **+3.42%** Top1 accuracy and **+3.90%** mAP, indicating the potential of scaling up the world models learned on feature space.

We also visualize the retrieving results in Figure 3. Representation methods like DoRA, which rely on only semantic similarities, always fail to retrieve future states when humans have large movements. On the contrary, after formulating the relation between egocentric observations and human skeletons, EgoAgent can predict the correct future state features, and then retrieve the real future image.

#### 4.5. Act: 3D Human Motion Prediction

We compare our method with state-of-the-art video-based motion generation Diffusion Policy [13] and human motion prediction models [23] using the egocentric human skeletons from Ego-Exo4D [21]. Every testing sample with time steps  $T_s = 4$  contains 4 frames of egocentric images and 20 frames of 3D human skeleton. To compare these two types of motion prediction models, we set the prediction targets as the last 15 frames of 3D human skeletons. 4 frames of egocentric images and the first 5 frames of 3D human skeletons are adopted as inputs for video-action models and human motion prediction models, respectively. For EgoAgent, both egocentric images and the first 5 frames of human skeletons are given to predict future actions. Following Ego-Exo4D [21], the mean per joint position error (MPJPE) in centimeters (cm) and the mean per joint velocity error (MPJVE) in centimeters per second (cm/s) for 3D joint positions and velocities are adopted as evaluation criteria.

**Results.** Quantitatively, as shown in Table 3, our EgoAgent-300M achieves state-of-the-art performance with the lowest MPJPE and competitive MPJVE. Specifically,



Figure 3. Retrieval results for egocentric future state prediction. Correct retrieval images are marked with green boundaries.

EgoAgent-300M improves the siMLPe [23] by **-0.41** and **-0.31** MPJPE (cm), on the evaluation set of 30fps and 10 fps, respectively. When scaling up EgoAgent to 1B, the prediction errors can be further decreased. These results demonstrate that world models can also predict actions accurately when given egocentric observations and past actions.

We also qualitatively evaluate the 3D human skeleton prediction results. As illustrated in Figure 4, given the starting 3D human skeleton, our EgoAgent shows relatively small errors compared with the ground truth. Compared with the video-based motion generation method Diffusion Policy [13], EgoAgent achieves better prediction accuracy on non-visible body keypoints. Specifically, on the beginning frame (see Figure 4  $t_2$ ), missing hands in the image leads to large prediction errors on Diffusion Policy, while EgoAgent learns from previous human motions and generates accurate predictions of the position of hands. Compared with motion-only motion generation methods, EgoAgent shows smaller accelerated errors. As shown in Figure 4  $t_3$ , after predicting several frames, the predicted skeletons start to lean against the floor. On the contrary, EgoAgent can integrate the information of the visible body parts in the egocentric observation and modify the accelerated errors.

#### 4.6. Ablation Study

To demonstrate the effectiveness of special designs in EgoAgent, we conduct several ablations with a short learning schedule of 14,400 iterations using EgoAgent-300M.

**Integration of represent, predict and act.** As EgoAgent achieves promising performance in representing, predicting, and acting, we explore how these three tasks influence

each other during training. We conduct leave-one-out experiments (as shown in Table 4), where we remove one task from the training process each time. First, removing any task will lead to worse performances, indicating that these three tasks, as foundation tasks of human learning from the world, can contribute to each other. Specifically, on video prediction tasks, removing the representation loss leads to a significant performance decrease with **-11.87%** Top1 and **-13.55%** mAP, demonstrating that representation is essential for predicting future states. Correspondingly, removing the prediction supervision also leads to the representation performance decrease of **-2.52%** and **-1.31%** Top1 accuracy on ImageNet-100 and ImageNet-1K, respectively. This result demonstrates that the representation ability can be strengthened by predicting future states, which is similar to the process of how humans learn from the world. Second, the motion prediction task is less sensitive to the removal of the representation learning task than the future state prediction task. This result indicates that EgoAgent can formulate the internal causal relationship between future state prediction and action prediction tasks, bringing additional improvement when jointly learning these two tasks.

**Train world model on feature space.** To ablate the effectiveness of training world models on feature space, we adopt a pretrained VQGAN [18] as the image tokenizer to formulate the entire task as the next-token prediction task on image and pose tokens. As shown in Table 4(d), training EgoAgent on the VQGAN latent space leads to significant performance drops on both future state prediction and image classification tasks, showing the effectiveness of train-

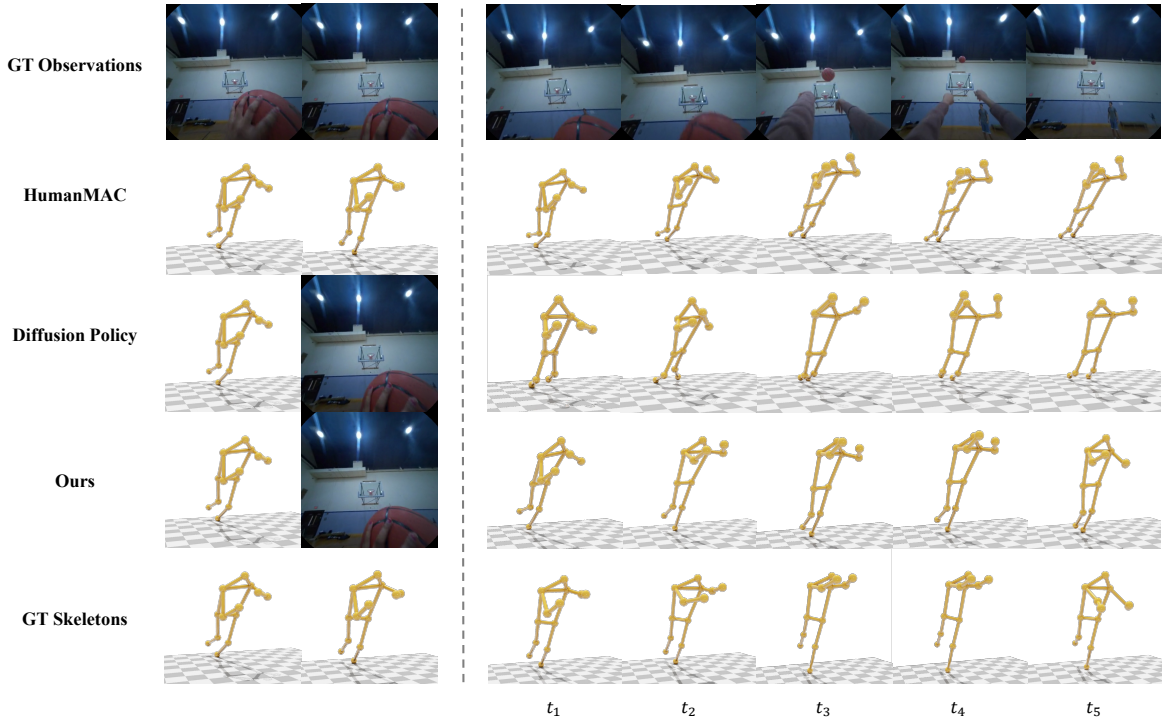


Figure 4. Visualizations of the 3D motion prediction tasks. After observing the egocentric frames, EgoAgent can generate accurate human skeletons even though most of the 3D body points are not visible in the input frame.

Table 4. Ablation of removing one task from the training and learning world in feature space. All variants are trained with 14,400 iterations.

Method	Tasks			Future State Prediction		Representation		Action Prediction	
	Represent	Predict	Act	Ego-Exo4D		ImgNet-100	ImgNet-1K	Ego-Exo4D (@30fps)	
				Top1	mAP	Top1	Top1	MPJPE ↓	MPJVE ↓
Baseline	✓	✓	✓	<b>37.77</b>	<b>53.72</b>	<b>41.64</b>	<b>22.28</b>	<b>14.49</b>	<b>88.61</b>
(a) w/o $\mathcal{L}_{rep}$		✓	✓	25.90	40.17	1.00	0.10	<b>14.49</b>	88.82
(b) w/o $\mathcal{L}_{pred}$	✓		✓	0.01	0.07	39.12	20.97	14.70	89.62
(c) w/o $\mathcal{L}_{act}$	✓	✓		34.86	49.13	39.92	21.31	107.03	-
(d) Latent		latent	✓	20.62	37.12	1.00	0.10	13.57	84.86

ing a world model on the feature space. We also find that the latent EgoAgent obtains better action prediction capabilities, which might be brought by the unification of task formulation. However, the performance drops on the other two tasks make training EgoAgent on the latent space not a desirable solution.

## 5. Conclusion and Limitations

In this paper, we presented EgoAgent, a joint predictive agent model designed to simultaneously learn to represent world observations, predict future states, and generate actions based on egocentric RGB input. EgoAgent integrates three critical abilities—perception, prediction, and interaction—within a unified transformer architecture. By align-

ing the representational spaces of these abilities and leveraging a teacher-student training mechanism, EgoAgent enables mutual reinforcement across tasks, facilitating improved learning and performance.

Through extensive experiments, we demonstrated that EgoAgent outperforms existing state-of-the-art methods in image classification, future state prediction, and 3D human motion prediction. However, we identify a key limitation as the sparse human skeleton representation, which excludes finger movements which are essential for precise tasks like object manipulation. Additionally, our model currently lacks long-term memory, limiting its ability to leverage historical context for tasks requiring extended temporal dependencies. Future work will explore further model improvements and scalability in more complex environments.



## References

- [1] Emre Aksan, Manuel Kaufmann, Peng Cao, and Otmar Hilliges. A spatio-temporal transformer for 3d human motion prediction. In *2021 International Conference on 3D Vision (3DV)*, pages 565–574. IEEE, 2021. 3
- [2] Eloi Alonso, Adam Jelley, Vincent Micheli, Anssi Kanervisto, Amos Storkey, Tim Pearce, and François Fleuret. Diffusion for world modeling: Visual details matter in atari. *arXiv preprint arXiv:2405.12399*, 2024. 2
- [3] Mahmoud Assran, Quentin Duval, Ishan Misra, Piotr Bojanowski, Pascal Vincent, Michael Rabbat, Yann LeCun, and Nicolas Ballas. Self-supervised learning from images with a joint-embedding predictive architecture. In *Proceedings of the IEEE/CVF Conference on Computer Vision and Pattern Recognition*, pages 15619–15629, 2023. 3
- [4] Jinze Bai, Shuai Bai, Yunfei Chu, Zeyu Cui, Kai Dang, Xiaodong Deng, Yang Fan, Wenbin Ge, Yu Han, Fei Huang, et al. Qwen technical report. *arXiv preprint arXiv:2309.16609*, 2023. 3
- [5] Chris Bamford and Simon M Lucas. Neural game engine: Accurate learning of generalizable forward models from pixels. In *2020 IEEE Conference on Games (CoG)*, pages 81–88. IEEE, 2020. 3
- [6] Adrien Bardes, Jean Ponce, and Yann LeCun. Mc-jepa: A joint-embedding predictive architecture for self-supervised learning of motion and content features. *arXiv preprint arXiv:2307.12698*, 2023. 3
- [7] Adrien Bardes, Quentin Garrido, Jean Ponce, Xinlei Chen, Michael Rabbat, Yann LeCun, Mahmoud Assran, and Nicolas Ballas. Revisiting feature prediction for learning visual representations from video. *arXiv preprint arXiv:2404.08471*, 2024. 3
- [8] Jake Bruce, Michael D Dennis, Ashley Edwards, Jack Parker-Holder, Yuge Shi, Edward Hughes, Matthew Lai, Aditi Mavalankar, Richie Steigerwald, Chris Apps, et al. Genie: Generative interactive environments. In *Forty-first International Conference on Machine Learning*, 2024. 4
- [9] Zhe Cao, Hang Gao, Karttikeya Mangalam, Qi-Zhi Cai, Minh Vo, and Jitendra Malik. Long-term human motion prediction with scene context. In *Computer Vision—ECCV 2020: 16th European Conference, Glasgow, UK, August 23–28, 2020, Proceedings, Part I 16*, pages 387–404. Springer, 2020. 2, 3
- [10] Mathilde Caron, Hugo Touvron, Ishan Misra, Hervé Jégou, Julien Mairal, Piotr Bojanowski, and Armand Joulin. Emerging properties in self-supervised vision transformers. In *Proceedings of the IEEE/CVF international conference on computer vision*, pages 9650–9660, 2021. 2, 4, 5, 6,
- [11] Ling-Hao Chen, Jiawei Zhang, Yewen Li, Yiren Pang, Xiaobo Xia, and Tongliang Liu. Humanmac: Masked motion completion for human motion prediction. In *Proceedings of the IEEE/CVF International Conference on Computer Vision*, pages 9544–9555, 2023. 6
- [12] Ting Chen, Simon Kornblith, Mohammad Norouzi, and Geoffrey Hinton. A simple framework for contrastive learning of visual representations. In *International conference on machine learning*, pages 1597–1607. PMLR, 2020. 2
- [13] Cheng Chi, Zhenjia Xu, Siyuan Feng, Eric Cousineau, Yilun Du, Benjamin Burchfiel, Russ Tedrake, and Shuran Song. Diffusion policy: Visuomotor policy learning via action diffusion. *The International Journal of Robotics Research*, page 02783649241273668, 2023. 6, 7
- [14] Enric Corona, Albert Pumarola, Guillem Alenya, and Francesc Moreno-Noguer. Context-aware human motion prediction. In *Proceedings of the IEEE/CVF conference on computer vision and pattern recognition*, pages 6992–7001, 2020. 3
- [15] Qiongjie Cui, Huaijiang Sun, and Fei Yang. Learning dynamic relationships for 3d human motion prediction. In *Proceedings of the IEEE/CVF conference on computer vision and pattern recognition*, pages 6519–6527, 2020. 3
- [16] Jia Deng, Wei Dong, Richard Socher, Li-Jia Li, Kai Li, and Li Fei-Fei. Imagenet: A large-scale hierarchical image database. In *2009 IEEE conference on computer vision and pattern recognition*, pages 248–255. Ieee, 2009. 2, 5
- [17] Alexey Dosovitskiy. An image is worth 16x16 words: Transformers for image recognition at scale. *arXiv preprint arXiv:2010.11929*, 2020. 4
- [18] Patrick Esser, Robin Rombach, and Bjorn Ommer. Taming transformers for high-resolution image synthesis. In *Proceedings of the IEEE/CVF conference on computer vision and pattern recognition*, pages 12873–12883, 2021. 7
- [19] Quentin Garrido, Mahmoud Assran, Nicolas Ballas, Adrien Bardes, Laurent Najman, and Yann LeCun. Learning and leveraging world models in visual representation learning. *arXiv preprint arXiv:2403.00504*, 2024. 3, 4
- [20] Kristen Grauman, Andrew Westbury, Eugene Byrne, Zachary Chavis, Antonino Furnari, Rohit Girdhar, Jackson Hamburger, Hao Jiang, Miao Liu, Xingyu Liu, et al. Ego4d: Around the world in 3,000 hours of egocentric video. In *Proceedings of the IEEE/CVF Conference on Computer Vision and Pattern Recognition*, pages 18995–19012, 2022. 2
- [21] Kristen Grauman, Andrew Westbury, Lorenzo Torresani, Kris Kitani, Jitendra Malik, Triantafyllos Afouras, Kumar Ashutosh, Vijay Baiyya, Siddhant Bansal, Bikram Boote, et al. Ego-Exo4D: Understanding skilled human activity from first- and third-person perspectives. In *Proceedings of the IEEE/CVF Conference on Computer Vision and Pattern Recognition*, pages 19383–19400, 2024. 2, 5, 6,
- [22] Jianyuan Guo, Zhiwei Hao, Chengcheng Wang, Yehui Tang, Han Wu, Han Hu, Kai Han, and Chang Xu. Data-efficient large vision models through sequential autoregression. *arXiv preprint arXiv:2402.04841*, 2024. 5
- [23] Wen Guo, Yuming Du, Xi Shen, Vincent Lepetit, Xavier Alameda-Pineda, and Francesc Moreno-Noguer. Back to mlp: A simple baseline for human motion prediction. In *Proceedings of the IEEE/CVF winter conference on applications of computer vision*, pages 4809–4819, 2023. 6, 7
- [24] David Ha and Jürgen Schmidhuber. Recurrent world models facilitate policy evolution. *Advances in neural information processing systems*, 31, 2018. 3
- [25] David Ha and Jürgen Schmidhuber. World models. *arXiv preprint arXiv:1803.10122*, 2018. 1, 2

- [26] Mohamed Hassan, Duygu Ceylan, Ruben Villegas, Jun Saito, Jimei Yang, Yi Zhou, and Michael J Black. Stochastic scene-aware motion prediction. In *Proceedings of the IEEE/CVF International Conference on Computer Vision*, pages 11374–11384, 2021. 3
- [27] Kaiming He, Xiangyu Zhang, Shaoqing Ren, and Jian Sun. Deep residual learning for image recognition. In *Proceedings of the IEEE conference on computer vision and pattern recognition*, pages 770–778, 2016. 2
- [28] Kaiming He, Haoqi Fan, Yuxin Wu, Saining Xie, and Ross Girshick. Momentum contrast for unsupervised visual representation learning. In *Proceedings of the IEEE/CVF conference on computer vision and pattern recognition*, pages 9729–9738, 2020. 2, 4
- [29] Kaiming He, Xinlei Chen, Saining Xie, Yanghao Li, Piotr Dollár, and Ross Girshick. Masked autoencoders are scalable vision learners. In *Proceedings of the IEEE/CVF conference on computer vision and pattern recognition*, pages 16000–16009, 2022. 2
- [30] Anthony Hu, Lloyd Russell, Hudson Yeo, Zak Murez, George Fedoseev, Alex Kendall, Jamie Shotton, and Gianluca Corrado. Gaia-1: A generative world model for autonomous driving. *arXiv preprint arXiv:2309.17080*, 2023. 3
- [31] Albert Q Jiang, Alexandre Sablayrolles, Antoine Roux, Arthur Mensch, Blanche Savary, Chris Bamford, Devendra Singh Chaplot, Diego de las Casas, Emma Bou Hanna, Florian Bressand, et al. Mixtral of experts. *arXiv preprint arXiv:2401.04088*, 2024. 3
- [32] Prannay Khosla, Piotr Teterwak, Chen Wang, Aaron Sarna, Yonglong Tian, Phillip Isola, Aaron Maschinot, Ce Liu, and Dilip Krishnan. Supervised contrastive learning. *Advances in neural information processing systems*, 33:18661–18673, 2020. 2
- [33] Yann LeCun. A path towards autonomous machine intelligence version 0.9. 2, 2022-06-27. *Open Review*, 62(1):1–62, 2022. 3
- [34] Zhenguang Liu, Kedi Lyu, Shuang Wu, Haipeng Chen, Yanbin Hao, and Shouling Ji. Aggregated multi-gans for controlled 3d human motion prediction. In *Proceedings of the AAAI conference on artificial intelligence*, pages 2225–2232, 2021. 3
- [35] I Loshchilov. Decoupled weight decay regularization. *arXiv preprint arXiv:1711.05101*, 2017.
- [36] Yecheng Jason Ma, Shagun Sodhani, Dinesh Jayaraman, Osbert Bastani, Vikash Kumar, and Amy Zhang. Vip: Towards universal visual reward and representation via value-implicit pre-training. *arXiv preprint arXiv:2210.00030*, 2022. 2, 5, 6
- [37] Takahiro Maeda and Norimichi Ukita. Motionaug: Augmentation with physical correction for human motion prediction. In *Proceedings of the IEEE/CVF Conference on Computer Vision and Pattern Recognition*, pages 6427–6436, 2022. 3
- [38] Arjun Majumdar, Karmesh Yadav, Sergio Arnaud, Jason Ma, Claire Chen, Sneha Silwal, Aryan Jain, Vincent-Pierre Berges, Tingfan Wu, Jay Vakil, et al. Where are we in the search for an artificial visual cortex for embodied intelligence? *Advances in Neural Information Processing Systems*, 36:655–677, 2023.
- [39] Wei Mao, Miaomiao Liu, and Mathieu Salzmann. Weakly-supervised action transition learning for stochastic human motion prediction. In *Proceedings of the IEEE/CVF Conference on Computer Vision and Pattern Recognition*, pages 8151–8160, 2022. 3
- [40] Julieta Martinez, Michael J Black, and Javier Romero. On human motion prediction using recurrent neural networks. In *Proceedings of the IEEE conference on computer vision and pattern recognition*, pages 2891–2900, 2017. 2
- [41] Russell Mendonca, Shikhar Bahl, and Deepak Pathak. Structured world models from human videos. *arXiv preprint arXiv:2308.10901*, 2023. 2, 3
- [42] Suraj Nair, Aravind Rajeswaran, Vikash Kumar, Chelsea Finn, and Abhinav Gupta. R3m: A universal visual representation for robot manipulation. *arXiv preprint arXiv:2203.12601*, 2022. 2, 5, 6
- [43] Tianxiang Sun, Xiaotian Zhang, Zhengfu He, Peng Li, Qinyuan Cheng, Xiangyang Liu, Hang Yan, Yunfan Shao, Qiong Tang, Shiduo Zhang, et al. Moss: An open conversational large language model. *Machine Intelligence Research*, pages 1–18, 2024. 3
- [44] InternLM Team. Internlm: A multilingual language model with progressively enhanced capabilities, 2023. 4,
- [45] Hugo Touvron, Thibaut Lavril, Gautier Izacard, Xavier Martinet, Marie-Anne Lachaux, Timothée Lacroix, Baptiste Rozière, Naman Goyal, Eric Hambro, Faisal Azhar, et al. Llama: Open and efficient foundation language models. *arXiv preprint arXiv:2302.13971*, 2023. 3
- [46] Aaron Van Den Oord, Oriol Vinyals, et al. Neural discrete representation learning. *Advances in neural information processing systems*, 30, 2017. 4
- [47] Shashanka Venkataramanan, Mamshad Nayeem Rizve, João Carreira, Yuki M Asano, and Yannis Avrithis. Is imagenet worth 1 video? learning strong image encoders from 1 long unlabelled video. *arXiv preprint arXiv:2310.08584*, 2023. 2, 5, 6,
- [48] Hongsong Wang, Jian Dong, Bin Cheng, and Jiashi Feng. Pvr: A position-velocity recurrent encoder-decoder for human motion prediction. *IEEE Transactions on Image Processing*, 30:6096–6106, 2021. 3
- [49] Jingbo Wang, Sijie Yan, Bo Dai, and Dahua Lin. Scene-aware generative network for human motion synthesis. In *Proceedings of the IEEE/CVF conference on computer vision and pattern recognition*, pages 12206–12215, 2021. 3
- [50] Yizhou Wang, Shixiang Tang, Feng Zhu, Lei Bai, Rui Zhao, Donglian Qi, and Wanli Ouyang. Revisiting the transferability of supervised pretraining: an mlp perspective. In *Proceedings of the IEEE/CVF Conference on Computer Vision and Pattern Recognition*, pages 9183–9193, 2022. 2
- [51] Yuqi Wang, Jiawei He, Lue Fan, Hongxin Li, Yuntao Chen, and Zhaoxiang Zhang. Driving into the future: Multiview visual forecasting and planning with world model for autonomous driving. In *Proceedings of the IEEE/CVF Conference on Computer Vision and Pattern Recognition*, pages 14749–14759, 2024. 3
- [52] Manuel Wüthrich, Felix Widmaier, Felix Grimminger, Joel Akpo, Shruti Joshi, Vaibhav Agrawal, Bilal Hammoud, Majid Khadiv, Miroslav Bogdanovic, Vincent Berenz, et al.

- Trifinger: An open-source robot for learning dexterity. *arXiv preprint arXiv:2008.03596*, 2020.
- [53] Jiannan Xiang, Guangyi Liu, Yi Gu, Qiyue Gao, Yuting Ning, Yuheng Zha, Zeyu Feng, Tianhua Tao, Shibo Hao, Yemin Shi, et al. Pandora: Towards general world model with natural language actions and video states. *arXiv preprint arXiv:2406.09455*, 2024. 2, 4
- [54] Weilai Xiang, Hongyu Yang, Di Huang, and Yunhong Wang. Denoising diffusion autoencoders are unified self-supervised learners. In *Proceedings of the IEEE/CVF International Conference on Computer Vision*, pages 15802–15812, 2023.
- [55] Hao Xue, Du Q Huynh, and Mark Reynolds. A location-velocity-temporal attention lstm model for pedestrian trajectory prediction. *IEEE Access*, 8:44576–44589, 2020. 3
- [56] Haitao Yan, Qiongjie Cui, Jiexin Xie, and Shijie Guo. Forecasting of 3d whole-body human poses with grasping objects. In *Proceedings of the IEEE/CVF Conference on Computer Vision and Pattern Recognition*, pages 1726–1736, 2024. 3
- [57] Mengjiao Yang, Yilun Du, Kamyar Ghasemipour, Jonathan Tompson, Dale Schuurmans, and Pieter Abbeel. Learning interactive real-world simulators. *arXiv preprint arXiv:2310.06114*, 2023. 2, 3, 4
- [58] Yufei Zhang, Jeffrey O Kephart, and Qiang Ji. Incorporating physics principles for precise human motion prediction. In *Proceedings of the IEEE/CVF Winter Conference on Applications of Computer Vision*, pages 6164–6174, 2024. 3
- [59] Yang Zheng, Yanchao Yang, Kaichun Mo, Jiaman Li, Tao Yu, Yebin Liu, C Karen Liu, and Leonidas J Guibas. Gimo: Gaze-informed human motion prediction in context. In *European Conference on Computer Vision*, pages 676–694. Springer, 2022. 3
- [60] Zangwei Zheng, Xiangyu Peng, Tianji Yang, Chenhui Shen, Shenggui Li, Hongxin Liu, Yukun Zhou, Tianyi Li, and Yang You. Open-sora: Democratizing efficient video production for all, 2024.

# Acquisition through My Eyes and Steps: A Joint Predictive Agent Model in Egocentric Worlds

## Supplementary Material

### 6. Additional Results on Embodied Tasks

To evaluate the broader applicability of our EgoAgent’s learned representation beyond video-conditioned 3D human motion prediction, we test its ability to improve visual policy learning for embodiments other than the human skeleton. Following the methodology in [38], we conduct experiments on the TriFinger benchmark [52], which involves a three-finger robot performing two tasks: reach cube and move cube. We freeze the pretrained representations and use a 3-layer MLP as the policy network, training each task with 100 demonstrations.

Table 5. Success rate (%) on the TriFinger benchmark, where each model’s pretrained representation is fixed, and additional linear layers are trained as the policy network.

Methods	Training Dataset	Reach Cube	Move Cube
DINO [10]	WT Venice	78.03	47.42
DoRA [47]	WT Venice	81.62	53.76
DoRA [47]	WT All	82.40	48.13
EgoAgent-300M	WT+Ego-Exo4D	82.61	54.21
EgoAgent-1B	WT+Ego-Exo4D	<b>85.72</b>	<b>57.66</b>

As shown in Table 5, EgoAgent achieves the highest success rates on both tasks, outperforming the best models from DoRA [47] with increases of +3.32% and +3.9% respectively. This result shows that by incorporating human action prediction into the learning process, EgoAgent demonstrates the ability to learn more effective representations that benefit both image classification and embodied manipulation tasks. This highlights the potential of leveraging human-centric motion data to bridge the gap between visual understanding and actionable policy learning.

### 7. Additional Results on Egocentric Future State Prediction

In this section, we provide additional qualitative results on the egocentric future state prediction task. Additionally, we describe our approach to finetune video diffusion model on the Ego-Exo4D dataset [21] and generate future video frames conditioned on initial frames as shown in Figure 5.

#### 7.1. Visualizations and Comparisons

More visualizations of our method, DoRA, and OpenSora in different scenes (as shown in Figure 6). For OpenSora, when predicting the states of  $t_k$ , we use all the ground truth frames from  $t_0$  to  $t_{k-1}$  as conditions. As OpenSora takes

only past observations as input and neglects human motion, it performs well only when the human has relatively small motions (see top cases in Figure 6), but can not adjust to large movements of the human body or quick viewpoint changes (see bottom cases in Figure 6).

#### 7.2. Finetuning OpenSora on Ego-Exo4D

OpenSora V1.1 [60], initially trained on internet videos and images, produces severely inconsistent results when directly applied to infer future videos on the Ego-Exo4D dataset, as illustrated in Figure 5. To address the gap between general internet content and egocentric video data, we fine-tune the official checkpoint on the Ego-Exo4D training set for 50 epochs. OpenSora V1.1 proposed a random mask strategy during training to enable video generation by image and video conditioning. We adopted the default masking rate, which applies: 75% with no masking, 2.5% with random masking of 1 frame to 1/4 of the total frames, 2.5% with masking at either the beginning or the end for 1 frame to 1/4 of the total frames, and 5% with random masking spanning 1 frame to 1/4 of the total frames at both the beginning and the end.

As shown in Fig. 5, despite being trained on a large dataset, OpenSora struggles to generalize to the Ego-Exo4D dataset, producing future video frames with minimal consistency relative to the conditioning frame. While fine-tuning improves temporal consistency, the moving trajectories of

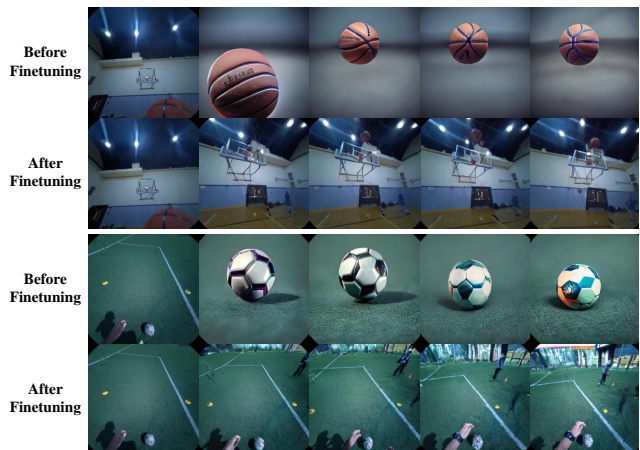


Figure 5. Comparison of OpenSora V1.1 first-frame-conditioned video generation results before and after finetuning on Ego-Exo4D. Fine-tuning enhances temporal consistency, but the predicted pixel-space future states still exhibit errors, such as inaccuracies in the basketball’s trajectory.



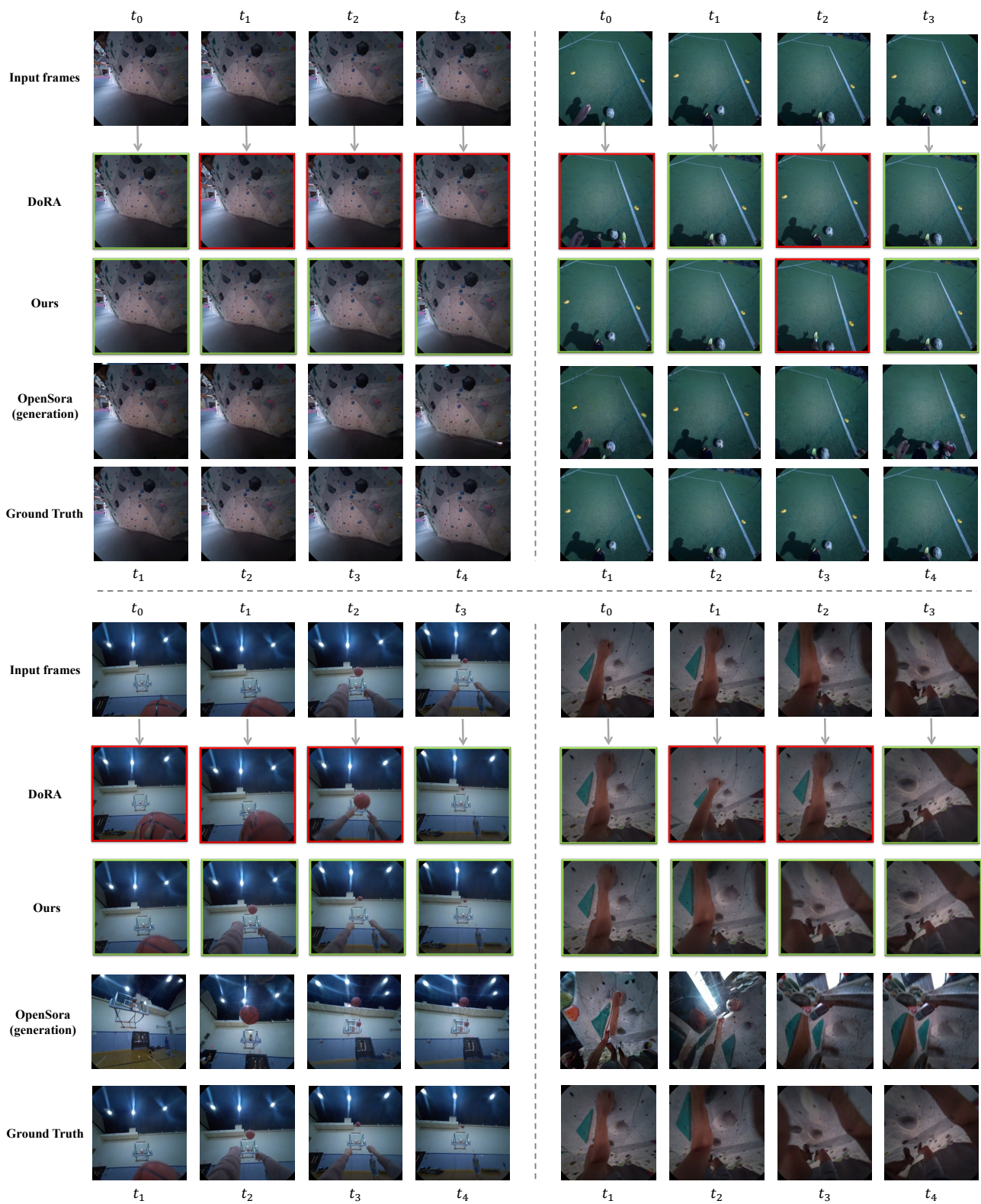


Figure 6. Retrieval and generation results for egocentric future state prediction. Correct and wrong retrieval images are marked with green and red boundaries, respectively.

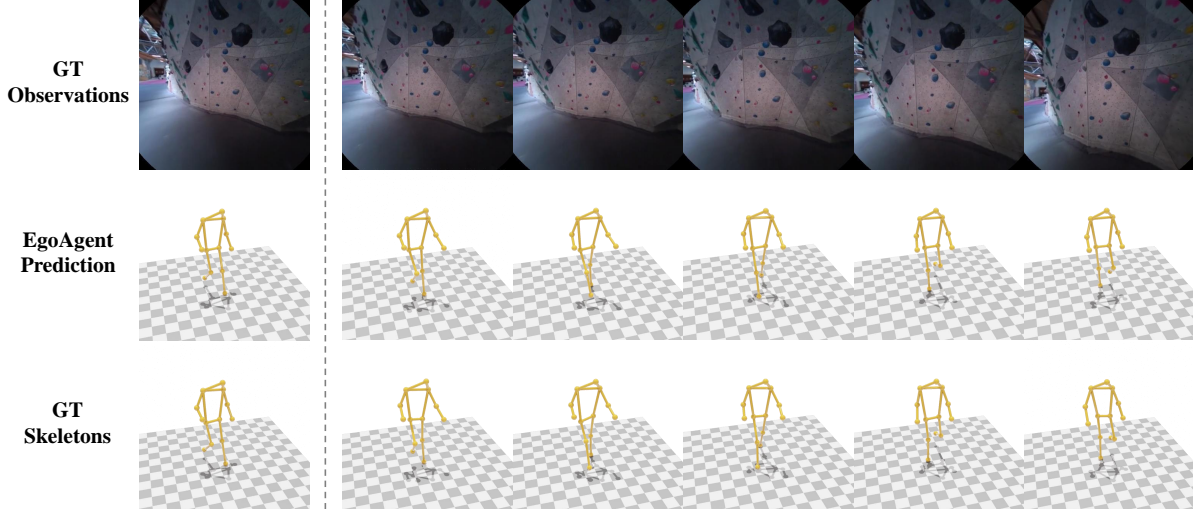


Figure 7. Motion prediction results in scenes with minor changes in observation.

objects like the basketball and soccer ball still deviate from realistic physical laws. Compared with our feature space prediction results, this suggests that training world models in a reconstructive latent space is more challenging than training them in a feature space.

## 8. Additional Results on 3D Human Motion Prediction

We present additional qualitative results for the 3D human motion prediction task, highlighting a particularly challenging scenario where egocentric observations exhibit minimal variation. This scenario poses significant difficulties for video-conditioned motion prediction, as the model must effectively capture and interpret subtle changes. As demonstrated in Fig. 7, EgoAgent successfully generates accurate predictions that closely align with the ground truth motion, showcasing its ability to handle fine-grained temporal dynamics and nuanced contextual cues.

## 9. OpenSora for Image Classification

In this section, we detail the process of extracting features from OpenSora V1.1 [60] (without fine-tuning) for an image classification task. Following the approach of [54], we leverage the insight that diffusion models can be interpreted as multi-level denoising autoencoders. These models inherently learn linearly separable representations within their intermediate layers, without relying on auxiliary encoders. The quality of the extracted features depends on both the layer depth and the noise level applied during extraction.

As shown in Table 6, we first evaluate  $k$ -NN classification performance on the ImageNet-100 dataset using three intermediate layers and five different noise scales. We find that a noise timestep of 128 yields the best results, with the

Table 6.  $k$ -NN evaluation results of OpenSora V1.1 features from different layer depths and noising scales on ImageNet-100. Top1 and Top5 accuracy (%) are reported.

Timesteps	First Layer		Middle Layer		Last Layer	
	Top1	Top5	Top1	Top5	Top1	Top5
32	6.10	18.20	34.04	59.50	30.40	55.74
64	6.12	18.48	36.04	61.84	31.80	57.06
128	5.84	18.14	38.08	64.16	33.44	58.42
256	5.60	16.58	30.34	56.38	28.14	52.32
512	3.66	11.70	6.24	17.62	7.24	19.44

middle and last layers performing significantly better than the first layer. We then test this optimal configuration on ImageNet-1K and find that the last layer with 128 noising timesteps achieves the best classification accuracy.

## 10. Data Preprocess

For egocentric video sequences, we utilize videos from the Ego-Exo4D [21] and WT [47] datasets. The original resolution of Ego-Exo4D videos is 1408×1408, captured at 30 fps. We sample one frame every five frames and use the original resolution to crop local views (224×224) for computing the self-supervised representation loss. For computing the prediction and action loss, the videos are downsampled to 224×224 resolution. WT primarily consists of 4K videos (3840×2160) recorded at 60 or 30 fps. Similar to Ego-Exo4D, we use the original resolution and downsample the frame rate to 6 fps for representation loss computation. As Ego-Exo4D employs fisheye cameras, we undistort the images to a pinhole camera model using the official Project Aria Tools to align them with the WT videos.

For motion sequences, the Ego-Exo4D dataset provides

synchronized 3D motion annotations and camera extrinsic parameters for various tasks and scenes. While some annotations are manually labeled, others are automatically generated using 3D motion estimation algorithms from multiple exocentric views. To maximize data utility and maintain high-quality annotations, manual labels are prioritized wherever available, and automated annotations are used only when manual labels are absent. Each pose is converted into the egocentric camera’s coordinate system using transformation matrices derived from the camera extrinsics. These matrices also enable the computation of trajectory vectors for each frame in a sequence. Beyond the x, y, z coordinates, a visibility dimension is appended to account for keypoints invisible to all exocentric views. Finally, a sliding window approach segments sequences into fixed-size windows to serve as input for the model. Note that we do not downsample the frame rate of 3D motions.

## 11. Training Details

### 11.1. Architecture Configurations

In Table 7, we provide detailed architecture configurations for EgoAgent following the scaling-up strategy of InternLM [44]. To ensure the generalization, we do not modify the internal modules in InternML, *i.e.*, we adopt the RMSNorm and 1D RoPE. We show that, without specific modules designed for vision tasks, EgoAgent can perform well on vision and action tasks.

Table 7. Architecture configurations of EgoAgent.

	EgoAgent-300M	EgoAgent-1B
Depth	22	22
Embedding dim	1024	2048
Number of heads	8	16
MLP ratio	8/3	8/3
#param.	284M	1.13B

Table 8 presents the detailed configuration of the embedding and prediction modules in EgoAgent, including the image projector ( $\text{Proj}_i$ ), representation head/state prediction head ( $\text{MLP}_i$ ), action projector ( $\text{Proj}_a$ ) and action prediction head ( $\text{MLP}_a$ ). Note that the representation head and the state prediction head share the same architecture but have distinct weights.

### 11.2. Training Configurations

In Table 9, we provide the detailed training hyper-parameters for experiments in the main manuscripts.

Table 8. Architecture of the embedding ( $\text{Proj}_i, \text{Proj}_a$ ) and prediction ( $\text{MLP}_i, \text{MLP}_a$ ) modules in EgoAgent. For details on module connections and functions, please refer to Fig. 2 in the main paper.

	Norm & Activation	Output Shape
<i>Proj<sub>i</sub> (Image projector)</i>		
Input image	-	3×224×224
Conv 2D (16×16)	-	Embedding dim×14×14
<i>MLP<sub>i</sub> (State prediction head &amp; Representation head)</i>		
Input embedding	-	Embedding dim
Linear	GELU	2048
Linear	GELU	2048
Linear	-	256
Linear	-	65536
<i>Proj<sub>a</sub> (Action projector)</i>		
Input pose sequence	-	4×5×17
Conv 2D (5×17)	LN, GELU	Embedding dim×1×1
<i>MLP<sub>a</sub> (Action prediction head)</i>		
Input embedding	-	Embedding dim×1×1
Linear	-	4×5×17

Table 9. Hyper-parameters for training EgoAgent.

Training Configuration	EgoAgent-300M/1B
Training recipe:	
optimizer	AdamW [35]
optimizer momentum	$\beta_1 = 0.9, \beta_2 = 0.999$
Learning hyper-parameters:	
base learning rate	6.0E-04
learning rate schedule	cosine
base weight decay	0.04
end weight decay	0.4
batch size	1920
training iters	72,000
lr warmup iters	1,800
warmup schedule	linear
gradient clip	1.0
data type	float16
norm epsilon	1.0E-06
EMA hyper-parameters:	
momentum	0.996